Epstein-Barr viral product-containing exosome facilitates LIF-associated immunosuppressive polarization of macrophage in nasopharyngeal carcinoma

Tzu-Tung Liu[1], Yun-Hua Sui[1], Shih-Sheng Jiang[2], Fang-Yu Tsai[2], Kai-Ping Chang[3], Ngan-Ming Tsang[4], Meng-Hsin Lee[1], Chen-Han Huang[1], Shu-Chen Liu[1*]

[1] Department of Biomedical Sciences and Engineering, National Central University, Taiwan

[2] Institute of Cancer Research, National Health Research Institutes, Taiwan

[3] Department of Otolaryngology-Head & Neck Surgery, Linkou Chang Gung Memorial Hospital, Taiwan

[4] Department of Radiation Oncology, China Medical University Hsinchu Hospital, Zhubei City, Hsinchu County, Taiwan

Keywords: Nasopharyngeal carcinoma, Epstein-Barr virus, exosome, tumor-associated macrophages, leukemia inhibitory factor, immune evasion, tumor microenvironment

Abstract

Nasopharyngeal carcinoma (NPC) is characterized by Epstein-Barr virus (EBV) infection and severe immune cell infiltration. How tumor-derived EBV or viral products regulate macrophage polarization within NPC microenvironment remains to be explored. Here, we investigated the exosome-mediated intercellular communications between EBV^+ NPC cells and tumor-associated macrophages (TAMs). We demonstrate that leukemia inhibitory factor (LIF) expression correlates with poorer metastasis/recurrence-free survival in NPC patients. Immunohistochemical analyses revealed that LIF is highly expressed by both tumor cells and macrophages. The uptake of NPC-derived exosomes by human monocyte-derived macrophages induced an immunosuppressive polarization and enhanced LIF expression, exhibiting a reduced cytotoxicity against primary cancer cells. Blocking LIF suppressed the pro-tumor functions mediated by tumor-derived exosomes, in both *in vitro* and *in vitro* zebrafish xenografts model. Furthermore, single-cell transcriptomic analysis (scRNA-seq) suggested that tumor-derived exosomes remodeled the NPC microenvironment by increasing the proportion of a pro-tumoral TAM subtype, CCL18-MΦ. Intercellular analysis revealed that exosome-treated macrophages could modulate T cell cytotoxicity and promoting Treg-mediated immunosuppression. Collectively, EBV shapes the tumor microenvironment by driving macrophage toward an immunosuppressive phenotype via exosome cargos, facilitating a pro-tumoral niche and contribute to NPC progression.

Introduction

Tumor-associated macrophages (TAMs) are the most abundant immune cells within tumors. TAMs play a pivotal role in creating an immunosuppressive tumor microenvironment (TME) and contribute to tumor progression by mediating tumor growth, invasion, and metastasis [1-5]. The infiltration of TAMs has been linked to poor prognosis in various cancers, including nasopharyngeal carcinoma (NPC) [6, 7]. Macrophages exhibit considerable plasticity and functional diversity in response to different stimuli. In the NPC TME, exosomes secreted by cancer cells carry a variety of molecules that have implications in intercellular communications and are critical for remodeling microenvironment. Evidence demonstrates that exosomes influence the differentiation, metabolic processes and functions of various cells, such as fibroblasts and immune cells [8-11], whereas the mechanisms underlying tumor-derived exosomes mediates macrophage polarization remain unclear.

Nasopharyngeal carcinoma (NPC) is a head and neck malignancy characterized by severe stromal and lymphocyte infiltration and high distant metastasis potential. The predominant association of NPC with Epstein-Barr virus (EBV) infection is a hallmark of this cancer. One of the key viral oncoproteins encoded by EBV is latent membrane protein-1 (LMP1), which mimics CD40, a member of the tumor necrosis factor receptor family, and activates signaling pathways through its C-terminal activating regions (CTARs). Numerous studies have shown that EBV develops immune escape mechanisms that assist cancer cells in creating a pro-tumor microenvironment [12-14]. For instance, LMP1 aids NPC

to evade immune surveillance by suppressing the activation and proliferation of T cells and natural killer cells [15, 16].

Our previous work highlighted the clinical significance of leukemia inhibitory factor (LIF) expressed by NPC cells [17]. Given that NF-κB signal activation by LMP1 leads to increased LIF expression and subsequent increased tumor growth in NPC, we sought to determine whether LMP1 reprograms TAMs through LIF to alter the microenvironment. Here, we investigated how the NPC-derived EBV product-containing exosomes influence the functions and polarization of macrophages. We found TAMs expressing LIF correlate with poor prognosis in NPC patients. Our data demonstrate that uptake of these exosomes by macrophages results in an immunosuppressive phenotype and LIF activation. We applied the single-cell RNA sequencing to dissect the expression patterns of macrophage subtypes and their interactions with neighboring populations within NPC TME. Further, exosome treatment partially suppresses T cell activation and promotes NPC cell growth. Notably, blocking LIF released by TAMs with sLIFR attenuates the exosome-mediated NPC progression *in vivo*. The present study suggests targeting LIF in NPC may limit the effects of tumor-derived exosomes fostering a tumor-promoting microenvironment and improve clinical outcomes.

Materials and Methods

Clinical samples

NPC formalin-fixed paraffin-embedded (FFPE) tumor tissues for IHC assays, fresh NPC tissues, and whole blood for single-cell RNA-seq were obtained from Linkou Chang Gung Memorial Hospital, Taiwan. Whole blood used for bulk RNA-seq experiments was obtained from healthy donors. All samples used in this study were under approval of the Institutional Review Board (IRB) of Chang Gung Medical Foundation.

Cell culture

HK1 EBV (EBV^+ human NPC cell line), HK1, B95-8 (EBV^+ B-lymphoblastoid cell line), AKATA (EBV^+ Burkitt's lymphoma cell line), BM1 (human NPC cell line) and THP-1 (human monocyte cell line) cells were cultured in RPMI-1640 medium supplemented with 10% fetal bovine serum (FBS) (Peak) and 1% penicillin-streptomycin (P/S) (Corning). TW06 (human NPC cell line) cells were growth in DMEM medium with 10% FBS and 1% P/S. Primary monocytes were isolated from PBMCs and cultured in α-MEM medium with 10% FBS and 1% P/S. primary head and neck cancer cells used in killing assays were cultured in defined KSFM medium (Gibco) containing growth factors and antibiotics. All cells were cultured under the condition of 37℃ and 5% CO2.

Exosome isolation and labeling

Exosomes were purified from the culture medium of EBV^+-NPC cells with SBI's ExoQuick-TC gradient solution (catalog# EXOTC50A-1) following the manufacturer's protocols. The collected exosome pellets were resuspended in cold PBS and stored at −80°C until use. For exosome labeling,

exosomes were fluorescent-labeled using ExoGlow™-Protein EV Labeling Kit (Green) (SBI, catalog# EXOGP300A-1) according to manufacturer's instructions. Briefly, 200µg exosomes in PBS were treated with labeling dye under shaking condition for 20 minutes. Labelled exosomes were then added with ExoQuick-TC solution and incubated at 4°C for 2 hours to 16 hours, followed by centrifugation and resuspension in PBS. The labelled exosomes were either immediately used or stored at −80°C. The protein-based labeling avoids non-specific signal aggregation and is capable of detecting single exosomes with low background.

Mass spectrometry (MS)-based proteomic analysis of exosomes

Proteomic profiling of exosomes was performed using a LC-ESI-MS/MS at Academia Sinica Common Mass Spectrometry Facilities, Taipei, Taiwan. 10µg exosome lysates were reduced with dithiothreitol (DTT) and alkylated using 55 mM iodoacetamide (IAM) in 50 mM ammonium bicarbonate for 45 minutes, followed by trypsin digestion and Zip Tip C18 desalting. 0.5µg protein digests were separated by a 90 minutes LC gradient then submitted to Orbitrap Elite MS (Thermo Fisher Scientific). For MS data interpretation, Proteome Discoverer (Thermo Fisher Scientific) was applied to process the raw data files and generate MGF files. Protein identification was performed using MSFragger search engine [18], against reviewed EBV database obtained from Uniport (August, 2022: 738 entries). Peptides with probability greater than 99% were accepted.

Transmission electron microscopy (TEM) of exosomes

Fresh isolated exosomes were mixed with anti-CD9 antibody (BD Pharmingen, 555370)-conjugated magnetic beads (Dynabeads M−270 Epoxy, Invitrogen) and incubated for 30 minutes, then the beads were blocked using 1% BSA/PBS. Following PBS wash, the exosome-captured beads were resuspended in PBS for imaging. Five µl of purified exosomes were transferred to a 200-mesh copper EM grid (Ted Pella), incubated at room temperature for 8 minutes and subsequently rinsed with distilled water. After that, the grid was applied to 1.5% w/v phosphotungstic acid (PTA) (Merck) for 3 seconds and washed again using distilled for negative staining. The visualization of exosomes was carried out using a TEM operating at 200 kV (JEM-2000 FX, JEOL).

Peripheral blood mononuclear cells (PBMCs) isolation

Peripheral blood mononuclear cells (PBMCs) were isolated using density gradient centrifugation method. Whole blood collected in a heparin-coated tube was diluted with 0.9% normal sodium and carefully underlaid with 15ml Ficoll-Paque gradient. The mixture was centrifuged at 400 xg for 40 min. PBMCs were isolated from the buffy coat layer, washed in PBS twice. Contaminated RBCs were removed by using RBC lysis buffer. The processed cells were resuspended in the desired concentration. Calcein-AM/PI double staining method was used to evaluate the viability of collected cell populations. Cell suspensions with viability greater than 90% were proceeded to library construction steps.

Differentiation of monocytes to macrophages

Freshly isolated or thawed PBMCs were grown in α-MEM medium in the presence of GM-CSF for 1.5 hours, followed by a wash, then cultured in α-MEM medium with 10% FBS. After 6 days, cells were stimulated with activation factors (50 ng/ml IFNγ and 10 ng/ml LPS for M1-like Mφ; 20 ng/ml IL-4 for M2-like Mφ; 5 ng/ml TGF-β for M2c Mφ; 10 ng/ml IL-6 for M2d Mφ; 30 μg/ml exosomes for exosomal stimulation). Macrophages without factor treatment were considered as M0 macrophages (Mock). Medium was renewed and cells were re-stimulated with activation factors on day 9.

For THP-1 cell line differentiation, THP-1 monocytes were induced into M0 macrophage using 100ng/ml phorbol 12-myristate 13-acetate (PMA) for 14-16 hours, after which the PMA-containing medium was replaced with RPMI medium with 10% FBS. Cells were further incubated for 3 days for differentiation. For M1-like and M2-like polarization, cells were treated with factors (50 ng/ml IFNγ and 10 ng/ml LPS for M1-like Mφ; 20 ng/ml IL-4 for M2-like Mφ) the day after PMA addition.

Bulk RNA sequencing

RNA library construction was conducted by using QIAseq UPX 3' transcriptome kit (Qiagen, catalog# 333088). 7ng purified RNA for each sample (n = 4 per group) was loaded into a plate with reverse transcription primers. RNAs with poly(A) tails were reverse transcribed with an oligo-dt primer containing a random Unique Molecular Index (UMI) and a fixed cell ID. Each cell was tagged with a unique ID and unique molecular index (UMI) was attached to each RNA molecule. After reverse transcription, the generated cDNA was pooled for subsequent steps, including amplification, fragmentation, end-repair, A-tailing and adapter ligation. Libraries were sequenced on an Novaseq PE150 system (Illumina).

Bulk transcriptome analysis

The FASTQ file was analyzed by QIAseq UPX 3' Transcriptome Primary Quantification tool (QIAGEN GeneGlobe analysis website) to generate gene expression matrix, which was further processed in R (version 4.0.3). Quality control was performed to remove genes whose number of samples with at least one UMI was fewer than half the sample number. Differential expressed analysis was performed by DESeq2 R package (version 1.30.1) [19], with adjusted P-value < 0.05 served as the cutoff value.

To explore differential activities of pathways between cells, gene set enrichment analysis (GSEA) was performed using the GSEA software (version 4.1.0) [20]). Differentially expressed gene lists were ranked by Signal2Noise calculated by the difference of means scaled by the standard deviation. Up and down regulated gene sets (Molecular Signatures Database [20]) were evaluated for enrichment score against the gene list. FDR < 0.25 was recognized as a differentially expressed threshold.

Single-cell suspension preparation

Fresh tissue samples were immediately washed and cut into small pieces (< 2-mm^3) after collection,

then processed with enzymatic digestion using a gentleMACS Dissociator (Miltenyi Biotec). The dissociated cells were neutralized by DMEM medium supplemented with 10% FBS and filtered through a 40 μm mesh to remove unwanted tissue and debris. Following RBC removal and wash steps (1100-1200 rpm, 6 minutes centrifugation), the processed cells were resuspended at the desired concentration. Additional debris removal (Miltenyi Biotec) was conducted if needed. Calcein-AM/PI double staining method was used to access the viability of collected cell populations. Cell suspensions with viability greater than 90% proceeded to library construction steps. Tissues and cells were kept on ice whenever possible during the entire procedure. For exosomal treatment experiments, processed cells were treated with 50μg exosomes for 2 hours under standard cell culture conditions (37°C and 5% CO2).

Single-cell RNA sequencing (scRNA-seq) and pre-processing

The scRNAseq libraries were generated using Chromium™ Single Cell 3' v3.1 Reagent Kit (10x Genomics) following the manufacturer's protocols. Briefly, oligonucleotide-barcoded cells were partitioned into single cell gel beads-in-emulsion (GEMs) using a microfluidics chip platform. Subsequent steps including reverse transcription and cDNA amplification were then conducted. Libraries were sequenced on NovaSeq 6000 Sequencing System (Illumina). The sequencing data were first processed using Cell Ranger's pipelines (version 6.1.2; 10x Genomics). In short, the raw binary base call (BCL) files were demultiplexed and converted to FASTQ files. Reads were then mapped to human genome reference sequence (GRCh38). Gene expression matrices were generated for downstream analysis. We used Seurat R package (version 5.1.0) [21] as the main tool for quality control, normalization, dimension reduction, clustering, and differential expression (DE) analysis. Cells with fewer than 200 or more than 8000 feature counts or over 10% mitochondrial genes were excluded to remove low-quality cells and cell multiplets. Doublets were further filtered by DoubletFinder (version 2.0.3) [22]. Expected doublet rate of each sample was determined based on the multiplet rate table provided by 10x Genomics. 4598 cells were excluded during quality control.

scRNA-seq pathway enrichment analysis

Signature scores were calculated by UCell R package (version 2.6.2) [23], with the gene lists are provided in Table S1. Additionally, we performed gene set variation analysis (GSVA) using GSVA R package (version 1.50.5) [24] to calculate enrichment scores for each cell. Hallmark gene sets and C2 curated gene sets (including KEGG, Reactome and CGP subsets) obtained from the Molecular Signatures Database (MSigDB) were used as reference datasets. To determine key pathways affected by radiation, we conducted t-tests comparing the exosome-treatment and control groups. P-values < 0.05 was recognized as a differentially expressed threshold.

scRNA-seq cell-cell communication analysis

We applied NicheNet (version 2.1.5) [25] approach to investigate interactions among cell populations.

Malignant cancer cells and TAMs were used as ligand resources (sender cells), and T cells were target (receiver) cells. Genes expressed in more than 5% of cells within each population were considered "expressed genes" for ligand activity analysis.

Quantitative real-time RT-PCR (qRT-PCR)

Total RNA was extracted using Qiagen RNA purification kit (catalog# 74536) following manufacturer's instructions. One ug of RNA was used for synthesis of complementary DNA (cDNA) by reverse transcription kit (Bio-Rad). The sequence extracted from Ensembl database was utilized to design primer sets for real-time PCR. All primer sequences are listed in Table S2. LightCycler probe design software was used for primer designation, and qRT-PCR was conducted using LightCycler 96 machine (Roche).

Western blotting

Cells and exosomes were lysed in lysis buffer containing 1mM PMSF, PhosSTOP™ Phosphatase Inhibitor (Roche, catalog# 4906837001) and cOmplete™ Protease Inhibitor Cocktail (Roche, catalog# 4693132001). After centrifugation and denaturation, equal amounts of proteins lysate were separated on SDS PAGE, then be transferred to PVDF membranes. 5% bovine serum albumin or 5% milk were subsequently used to block non-specific proteins. Next, membranes were incubated in 5% BST/TBST containing specific primary antibodies against target proteins, followed by secondary antibody conjugated to horseradish peroxidase (HRP). Bands were visualized with enhanced chemiluminescence (ECL) reagents.

Zebrafish embryonic xenograft model

The wild-type and Tg (flila: EGFP) y1 transgenic zebrafish strains were purchased from Taiwan Zebrafish Core Facility at National Health Research Institutes (NHRI). For the microinjection experiment, 300-400 human NPC cells (TW06_RFP) suspended in approximately 5 nl PBS were injected into the yolk sac of embryos immediately after the retrieval of eggs (within 30 minutes after fertilization). All cells were washed with cold PBS at least three times before injection and kept on ice whenever possible during the process. Injected fish were maintained at 37 °C, with the temperature elevated at the speed of 1°C / 6 hours starting from 28°C. Tumor xenografts in living fish were measured by Olympus IX83 microscopy and analyzed using Olympus CellSens software.

Real-time cell analyzer (RTCA) xCELLigence assay

To assess the influence of conditioned medium (CM) of macrophages on NPC cell growth, we used the xCELLigence real-time analyzer (ACEA Biosciences) to monitor cellular impedance every 10 minutes for up to 6 days. 3-5 × 10^3 cells/well were seeded in a 96-well E-plate and treated with conditioned medium or 1ug/ml sLIFR (abcam, catalog#ab155609) at the specified time point. Cell index (CI) was normalized 1h prior to CM addition.

5-Ethynyl-2-deoxyuridine (EdU) incorporation assay

The Click-iT EdU assay (Thermo Fisher Scientific) was used to detected the proliferation ability of NPC cancer cells. Approximately 15000 TW06 cells/well were incubated for 24 hours, and then treated with condition medium (macrophage supernatant) or PBS control for 14 hours, followed by 10μM EdU labeling for an additional 4 hours. After 4% paraformaldehyde fixation, nuclei were stained with Hoechst 33342 (DAPI). The proliferating cells were observed by Olympus IX83 microscopy and analyzed using Olympus CellSens software.

Immunocytochemistry (ICC) staining

Macrophages were grown on the glass coverslips and fixed with 4% paraformaldehyde (PFA) in PBS. Following fixation, cells were permeabilized using 0.03% Triton X-100 in 3% BSA, and then blocked in 8% goat serum and Fc blocker, respectively. Primary antibodies were incubated at 4°C for overnight. Secondary antibodies conjugated with fluorescent dye were used at a dilution of 1:1000 for protein visualization. Hoechst 33342 DNA dye was used for nuclear staining.

Immunohistochemistry (IHC)

IHC staining for NPC FFPE tumor sections was performed by Novolink detection systems (Leica, RE7280) according to manufacturer's instructions. Tissues were deparaffinized and rehydrated in xylene substitute and graded ethanol respectively. Heat-induced antigen retrieval was achieved in 10mM citrate buffer (Leica, pH 6.0) or 1mM Tris-EDTA (pH 9.0) for 3 minutes. Sections were blocked with Novocastra Protein Block buffer and incubated with primary antibodies for 90 min at room temperature. After endogenous peroxidase blocking, sections were incubated with secondary antibodies (Leica Novolink Polymer or Scytek PAM015 PolyTek Polymerized HRP). For signal detection, the reaction was developed by diaminobenzene (DAB) and counterstained with hematoxylin. The stained sections were captured using Olympus IX83 microscopy.

Immunofluorescence (IF) imaging for tissue sections

Immunofluorescence staining was conducted to evaluate proteins colocalization in NPC FFPE sections. Deparaffinization, rehydration and antigen retrieval steps followed the same protocol as the IHC procedure. The sections were fixed with 4% PFA in PBS, permeabilized using 0.03% Triton X-100 in 3% BSA, and blocked with protein block reagent (HK112, BioGenex). Antibody incubation steps were carried out as described for ICC staining.

In situ hybridization (ISH)

We applied in situ hybridization assay detect EBERs expression in NPC sections with RNAscope 2.5 HD Kit (Advanced Cell Diagnostics, catalog# 322310) following the manufacturer's protocols. Tissues were hybridized with the EBER1 probe (GenBank Accession Number: KP195701) at 40°C for 2 hours, followed by amplification and detection. Images were captured using Olympus IX83 microscopy.

Antibodies

antibodies used in western blotting includes LMP1 (Kerafast, ETU001, RRID: AB_2938990, 1:3000), CD9 (Abcam, ab92726, RRID: AB_10561589, 1:1000), HSP70 (System Biosciences, EXOAB-HSP70A-1, RRID: AB_2687468, 1:4000), calnexin (Cell Signaling, #2679, RRID: AB_2228381, 1:1000), β-actin (Sigma, A5060, RRID: AB_476738, 1:8000), GAPDH (Abcam, ab9484, RRID: AB_307274, 1:5000), CD206 (Abcam, ab64693, RRID: AB_1523910, 1:1000), DC-SIGN (BD Biosciences, MAB161, RRID: AB_357808, 1:1000), VEGF (ABclonal, A17877, RRID: AB_2861741, 1:500), CD86 (Cell Signaling, #91882, RRID: AB_2797422, 1:1000), LIF(Abgent, AP6981c, RRID:AB_1967900, 1:1000), phospho-IκBα (Abcam, ab97783, RRID: AB_10680152, 1:2000), IκBα (Santa Cruz Biotechnology, sc-371, RRID: AB_2235952, 1:2000), phospho-AKT (Cell Signaling, 9271, RRID: AB_329825, 1:1000), AKT (Epitomics, 1085, RRID: AB_562034, 1:3000), phospho-STAT3 (Cell Signaling, 9145, RRID: AB_2491009, 1:2000), STAT3 (Santa Cruz Biotechnology, sc-482, RRID: AB_632440, 1:500). Primary antibodies against the following proteins were applied in IHC or ICC: LIF (Abcam, ab135629, 1:80), LMP1 (Kerafast, ETU001, RRID: AB_2938990, 1:50), EBV early antigen D (EaD; Abcam, ab30541, RRID: AB_732194, 1:150), CD68 (Abcam, ab213363, RRID: AB_2801637, 1:7000; Santa Cruz Biotechnology, sc-20060, RRID: AB_627158, 1:80), iNOS (Abcam, ab178945, RRID: AB_2861417, 1:25)

Statistical analysis

Statistical analyses were conducted using R or GraphPad Prism 10 (GraphPad Software). Two-tailed Comparisons between two groups of experimental measurements were performed using a two-tailed Student's *t* test. For multiple group comparisons, one-way Analysis of Variance (ANOVA) with Benjamini-Hochberg correction was applied. Mann–Whitney *U* test was used to estimate differences between clinical samples. Kaplan-Meier recurrence-free and metastasis-free survival were used to compare survival times between groups based on IHC scores. Statistical significance was determined for differences at *p*-value below 0.05.

Data availability

The processed and raw single-cell data generated in this study were deposited in the Gene Expression Omnibus (GEO) (GSE280127). The bulk RNA sequencing data generated in this study are available under the accession number GSE282685.

Results

LIF expression correlates with poor prognosis in NPC

LIF is increasingly recognized for its pivotal role in tumorigenesis and immune modulation [26-28]. Our previous studies reported an association between LIF levels and NPC progression. Immunohistochemical analyses revealed that LIF expression significantly correlates with both poorer

recurrence-free and metastasis-free survival. NPC patients diagnosed with distant metastasis exhibited significantly stronger LIF expression compared to those without metastasis (Fig.1A, B). Additionally, we observed that the staining pattern of LIF was not restricted to tumor cells but resembles that of immune cells. To further investigate its immunological significance, we analyzed LIF expression in various immune populations, including T cells, macrophages, mast cells, and neutrophils, by examining its colocalization with specific cell type markers. Beyond its presence in tumor cells, we found that LIF is also expressed by $CD68^+$ macrophages (Fig.1C, D). Additionally, LIF-expressing TAMs were more abundant around the tumors with an M2-like phenotype compared to TAMs within the tumor core (Fig 1D). These IHC analyses indicate the colocalization of LIF and CD68, along with their correlation with poor prognosis in NPC patients, suggesting TAM infiltration may be significantly involved in NPC development.

Detection of EBV-encoded products in NPC sections.

We examined the presence of EBV in FFPE NPC tissue by detecting expressions of EBV-encoded small RNAs (EBERs), EBV early antigen D (EaD) and latent membrane protein 1 (LMP1) (Fig.2A). Positive expressions of EBERs and EaD were detected in most NPC samples tested (62/66). Notably, in the vicinity of $EBER^+$ tumors, a bunch of $EBERs^+$ vesicle-like structures were scattering into matrix of TME, and some stromal immune cells along the vesicle tracks were EBERs positive (Fig.2B). We speculated that EBV might load its viral products into the vesicle-like structures and release them into matrix, and the uptake of these vesicles by certain types of immune cells could alter tumor immunity. Prior studies have demonstrated LMP1 serves as one of the most important EB oncogenes that assist cancer cells in creating an immunosuppressive and pro-tumor microenvironment [12-14]. Our IHC analyses showed that LMP1 can be detected in both adjacent normal tissues and tumor areas (Fig.2C). The presence of LMP1 in both tumors and adjacent normal tissues suggests that LMP1 from tumor cells may influence nearby non-cancerous cells, potentially facilitating tumor progression and immune evasion. EBV-related exosomes are capable of transferring viral products such as LMP1 within the tumor microenvironment, thereby promoting oncogenic signaling in neighboring cells. To address whether LMP1 plays a pivotal role in influencing macrophages in TME, we performed immunofluorescence double staining for LMP1 and pan-macrophage marker (CD68) in human NPC sections (Fig.2D). LMP1 appeared as dot-like staining patterns on the cell membrane or in the cytoplasm, where it colocalized with CD68, indicating its presence in macrophages within the microenvironment.

EBV^+ NPC-derived exosomes induce macrophage immunosuppressive polarization and assist tumor growth

To investigate whether NPC cells mediate macrophage differentiation through exosomes, we isolated monocytes from primary human PBMCs and differentiated them into macrophage subtypes with different activation factors or EBV^+ NPC-derived exosomes (Fig.4A, also see Materials and Methods).

The structure of exosomes was verified by transmission electron microscopy (TEM) using CD9 antibody-coated magnetic beads to capture exosomes. TEM imaging identified exosomes as vesicles with sizes ranging from 50 to 150 nm in diameter (Fig.3A). Exosomal content was characterized by qualitative mass spectrometry (MS) and western blotting (Table S3 and Fig.3B). LMP1 and other EBV protein products such as EBNAs were identified in exosomes. In addition, to confirm that exosomes were engulfed by macrophages, we conducted time-lapse microscopy to monitor the process of exosome uptake (Fig.3C). The internalization of exosomes by macrophages was evident at 2 hours post exosome stimulation and continued to accumulate within the cells. Immunofluorescence detection of LMP1 and CD68 in macrophages treated with EBV product-containing exosomes revealed the presence of LMP1 within macrophages, also highlighting the its role in macrophage polarization.

Our results further showed that exosome treatment induced morphological changes in macrophages. Phenotypic changes were observed on day 9 post differentiation, M1-like group exhibited a rounded and flattened phenotype while M2-ilke and M2d groups were more elongated. In the exosomes treated cells, cells displayed a M2d-like morphology (Fig.4A). We next conducted transcriptomic analysis on subtypes of macrophages, profiling a total of 10313 genes after quality control. Principal component analysis (PCA) and heatmap clustering revealed that exosome-treated macrophages had a pattern more similar to that of M2d macrophages (Fig.4B, C). Macrophages exposed to exosomes expressed lower pro-inflammatory markers and higher immunoregulatory genes. Furthermore, these exosomes also partially reduced the antigen presentation capability of macrophages compared to M1-like phenotype (Fig.4C). qRT-PCR, western blotting and immunofluorescence staining were used to estimate the expression of pro-inflammatory and immunosuppressive genes, in order to further validate our sequencing data. As expected, M1-like, M2-like and M2d macrophages exhibited high levels ofCD86, CD206, and VEGF, respectively. Macrophages stimulated with exosomes expressed higher CD206 and VEGF, along with lower CD86 expression, resembling that of M2d macrophages (Fig.4D, E).

To investigate whether treating macrophages with tumor-derived exosomes affects their innate immune function, we conducted time-lapse microscopy to monitor the phagocytic ability of macrophages cocultivated with primary head and neck cancer cells. Cancer cells were added into the culture medium of macrophages after differentiation. As shown in Figure 4H, the phagocytic events by M0 macrophages (control group) could be observed at 30 hours post addition of cancer cells. In contrast, the cancer cells appeared to escape from exosome-treated macrophages. Additionally, the exosome-treated macrophages rarely contacted with cancer cells. Our data indicate that these exosomes may facilitate cancer immune evasion. The impact of exosomes on cancer cells proliferation was further assessed by real time cell analyzer (RTCA) and EdU incorporation analysis. TW06 (human NPC cell lines) cells were stimulated with supernatants harvested from different types macrophages (conditioned medium, CM). By measuring cell impedance using RTCA, we found exposure to exo-treated $M\varphi^{CM}$ enhanced the proliferation of NPC cells, whereas CM from untreated macrophages or M1-like, M2-like and M2d types resulted in relatively lower tumor cell growth. (Fig. 4F-G). Similarly,

exosomes led to an increase in the proportion of EdU-positive cells compared to the control group ($p < 0.001$) (Fig. 4I), suggesting that EBV product-containing exosomes mediate NPC cell proliferation.

LIF is associated with the immunosuppressive polarization of TAMs by EB product-containing exosomes

LIF has recently been implicated in the modulation of immune cells and poor prognosis in NPC. Here we assessed the role of LIF in the exosome-induced shifts in macrophage phenotype that contribute to tumor progression. We differentiated human PBMCs to macrophages with EBV^+ HK1 cells-derived exosomes (30 μg/ml). Exosomal stimulation enhanced the expression of LIF and pro-tumor markers CD206 and VEGF. LIF Promoter assay and western blot analysis of several LMP1 downstream target genes indicated that LMP1 might induced LIF activation through NFKB signaling (Fig.5A). Structurally, LMP1 consists of six transmembrane domains, a short N-terminal domain and a long C-terminal domain which comprises c-terminal activating regions (CTARs). It has been established that CTARs are main drivers for most LMP1-mediated signalings. By transfecting THP-1-derived macrophages with various LMP1 deletion mutants, we found the CTAR1 domain of LMP1 is required for the LIF activation. Mutant CTAR1 domain (mCTAR1) or C-terminus (ΔCterm), but not deleted CTAR2 (rCTAR2) abrogated the LMP1-mediated LIF enhancement.

The exosome-induced proliferation of NPC cells and effects of sLIFR were further validated by a real-time analyzer (RTCA) and an *in vivo* zebrafish model. In comparison with conditioned medium from M0 macrophages ($CM^{M\Phi}$), conditioned medium from exosome-treated macrophages (Exo-Tx $CM^{M\Phi}$) resulted in greater NPC cell growth, according to RTCA results, and this enhancement was suppressed by sLIFR (Fig.5C, D). For the zebrafish embryonic xenograft model, we injected NPC cells expressing red fluorescent protein (TW06_RFP), which treated with or without conditioned medium into the yolk sac of embryos of Tg (flia:EGFP) y1 zebrafish. The tumor xenografts and blood vessels of larvae could be observed under fluorescence microscopy on day 6-8 post injection. The results suggested that injecting NPC cells along with $CM^{M\Phi}$ defected the formation of tumor-like structure compared to fish injected with cancer cells alone (tumor area decreased from 4366 μm^2 to 2802 μm^2). However, the conditioned medium from exosome-treated macrophages (Exo-Tx $CM^{M\Phi}$) led to a greater tumor area. Importantly, treating cells with sLIFR partially rescued this effect of EBV^+ exosomes (from 3280 μm^2 to 1771 μm^2) by blocking LIF in the conditioned medium. Similar results were observed when analyzing dissemination and metastasis of tumor cells. In larvae injected with NPC cells combined with $CM^{M\Phi}$, Exo-Tx $CM^{M\Phi}$, and sLIFR-treated group (Exo-Tx $CM^{M\Phi}$ +sLIFR), the average numbers of metastasis-like structures were 2.6, 4.0 and 2.2, respectively. Together, these data suggest a potential role of LIF and exosome-treated macrophages in promoting tumor dissemination and metastasis, while sLIFR treatment attenuates these effects (Fig.6E-G).

Single-cell transcriptomic analysis uncovered microenvironment remodeled by NPC-derived exosomes.

The effect of tumor-derived exosomes on NPC microenvironment was further explored using single-

cell RNA sequencing (scRNA-seq). We investigated the phenotypic and functional alterations in macrophages, as well as exosome-induced cellular interactions. Cells were dissociated from a human NPC tissue and stimulated with exosomes from EBV^+ NPC cell lines (HK1EBV exo) for 2 hours. A total of 14,446 qualified cells were subjected to analysis. We identified epithelial cells, fibroblasts and 7 major types of immune repertoire, comprising myeloid cells, T/NK cells, B cells, mast cells and neutrophiles. Subtypes of immune cells were further identified based on expression of specific marker genes (Fig. 6A-C and Table S4). Among the three distinct subpopulations of TAMs, CCL18-MΦ exhibited relatively higher expression of FUCA1, CCL18, and ferroportin-associated genes SLC40A1 and SELENOP (SEPP1), which are known to promote tumorigenesis and M2-like polarization [29, 30]. SPP1-MΦ (SPP1, VCAN, INHBA) was identified as a pro-angiogenic population [31], while CXCL10-MΦ exerted pro-inflammatory effect by releasing CXCL10, CLEC10A and antigen presentation-related CD1 molecules. Notably, we found exosome treatment increased the proportion of CCL18-MΦ from 17.6% to 31.5%, implying that exosomes may contribute to the recruitment and expansion of macrophages involved in tumorigenesis (Fig.6E). To understand the functional impact of TAMs in response to exosomes, we analyzed key aspects of immune pathways, including antigen presentation, immune regulation, phagocytosis, and metabolism-related signalings. UCell and GSVA pathway analyses demonstrated that EBV product-containing exosomes increased CD163-mediated anti-inflammatory responses and enhanced pro-tumor activity through VEGF signaling, suggesting they induced a pro-tumoral and immunosuppressive phenotype (Fig. 6 D, F and G).

We next applied NicheNet to identify ligand-receptor activity and predicted target genes among different cell populations. Specifically, we focused on the cellular interactions between TAMs, malignant cells (as senders) and T cells (receivers), which are also highly infiltrated in TME. This approach allowed us to investigate the underlying mechanisms induced by NPC-derived exosomes. Results identified TGFB1, PD-L1 (CD274) and IL-6 expressed by TAMs and cancer cells may contribute to impaired anti-tumor immunity by interacting with T cells. The predicted downstream targets include HSPE1, a stress-induced chaperone protein associated with Tregs. HSPE1 was significantly elevated in exosome-treated samples, suggesting that EBV product-containing exosomes play a role in promoting Treg-mediated immunosuppression (Fig 6C). Figure 6E highlights differentially expressed genes involved in key T cell functional pathways across T cell subpopulations. In exosome-treated samples, cytotoxic genes GZMM and co-stimulatory markers (TNFRSF18, TNFRSF9) were notably downregulated in CTLs and $CD8^+$ exhausted T cells. Immune regulatory genes, including CTLA4, SOCS1and TIGIT, were upregulated in most CD4 and CD8 T cells. GSVA analysis further demonstrated alterations in in critical pathways and immunoregulatory interactions with non-lymphoid cells. Exosome treatment was shown to increase PD-1 signaling and suppress TCR signaling, particularly in CD4+ helper T cells and CD8+ exhausted T cells, further supporting the role of EBV^+ exosomes in dampening anti-tumor immunity. Together, these results suggest that EBV exosomes modulate the tumor-immune microenvironment by enhancing immunosuppressive signaling, promoting immune evasion, and facilitating NPC progression.

Discussion

Collectively, our data indicate that exosomes carrying LMP1 drive macrophage polarization toward an immunosuppressive phenotype through NFκB signaling and LIF induction. Here, we discussed the role of EBV product-containing exosomes in modulating macrophage immune responses, uncovering an underlying mechanism that illustrates how EBV^+ exosomes-driven pro-tumor microenvironment develops. Since TAMs play a critical role in remodeling TME, targeting signalings or key factors such as LIF may provide a potential approach for improving cancer treatment and prevention.

Several EBV-encoded products can be transferred to surrounding recipient cells via exosomes released by NPC cells, as demonstrated by our qRT-PCR data (Fig.3E). Among them, LMP1 is the most widely investigated viral oncogene in EBV-driven tumors, it not only plays a critical role in promoting cancer cell proliferation and transformation but also significantly impacts other cells within the TME. As a constitutively active receptor, LMP1 is able to induce a wide range of cellular responses by hijacking signaling pathways such as NF-κB, JAK/STAT3, and PI3K/AKT, without requiring a ligand. Given its high expression in immune cells like B cells, LMP1 has evolved effective strategies for immune evasion. Understanding the mechanisms is essential for the development of immunotherapies against EBV-related malignancies.

We aim to dissect the NPC microenvironment affected by EBV. Our studies have shown that LIF levels in either tumor cells or TAMs predict local recurrence and metastasis in NPC. LMP1 has the potential to activate LIF through CTAR1-NFκB signaling, promoting NPC tumorigenesis, radioresistance [17] and immune suppression. LIF/LIFR signals in cancer cells or LIF secreted by TAMs can be therapeutic targets and serve as circulating markers to improve clinical outcomes. In addition, EBV-related exosomes enhance the fibrotic response by activating YAP1 signaling in fibroblasts, thus contributing to a more proinvasive tumor stroma [32]. We also found that EBV utilizes adipocytes as a viral reservoir, regulating lipid metabolism to benefit virus persistence [33]. The single-cell transcriptomic model used in this study aided us in gaining deeper insights into tumor-stroma interplay in NPC with a focus on the impact of EBV product-containing exosomes. Our analyses reveal that malignant cells and TAMs tend to express higher levels of IL-6 and CD274, promoting Tregs differentiation through HSPE1 under exosome stimulation. Furthermore, we identified UBD, RAET1L, and the inhibitor of apoptosis (IAP) genes BIRC3 (cIAP2) and BIRC5 were significantly differentially expressed by malignant cells, which could serve as potential targets for reversing the effects of EBV. Taken together, we have discussed the involvement of EBV-encoded products in NPC progression and immune modulation, offering a deeper understanding of how these products shape the tumor microenvironment.

Reference

1. Cassetta, L. and J.W. Pollard, *Targeting macrophages: therapeutic approaches in cancer.* Nat Rev Drug Discov, 2018. **17**(12): p. 887-904.
2. Chen, Y., et al., *Tumor-associated macrophages: an accomplice in solid tumor progression.* Journal of Biomedical Science, 2019. **26**(1): p. 78.
3. Lin, Y., J. Xu, and H. Lan, *Tumor-associated macrophages in tumor metastasis: biological roles and clinical therapeutic applications.* Journal of Hematology & Oncology, 2019. **12**(1): p. 76.
4. Qian, B.-Z. and J.W. Pollard, *Macrophage Diversity Enhances Tumor Progression and Metastasis.* Cell, 2010. **141**(1): p. 39-51.
5. Ruffell, B. and L.M. Coussens, *Macrophages and therapeutic resistance in cancer.* Cancer Cell, 2015. **27**(4): p. 462-72.
6. Chen, Y.L., *Prognostic significance of tumor-associated macrophages in patients with nasopharyngeal carcinoma: A meta-analysis.* Medicine (Baltimore), 2020. **99**(39): p. e21999.
7. Huang, D., et al., *Epstein-Barr Virus-Induced VEGF and GM-CSF Drive Nasopharyngeal Carcinoma Metastasis via Recruitment and Activation of Macrophages.* Cancer Res, 2017. **77**(13): p. 3591-3604.
8. Buzas, E.I., *The roles of extracellular vesicles in the immune system.* Nature Reviews Immunology, 2023. **23**(4): p. 236-250.
9. Li, I. and B.Y. Nabet, *Exosomes in the tumor microenvironment as mediators of cancer therapy resistance.* Mol Cancer, 2019. **18**(1): p. 32.
10. Webber, J., et al., *Cancer Exosomes Trigger Fibroblast to Myofibroblast Differentiation.* Cancer Research, 2010. **70**(23): p. 9621-9630.
11. Zhu, D., et al., *Macrophage M2 polarization induced by exosomes from adipose-derived stem cells contributes to the exosomal proangiogenic effect on mouse ischemic hindlimb.* Stem Cell Res Ther, 2020. **11**(1): p. 162.
12. Albanese, M., et al., *MicroRNAs of Epstein-Barr Virus Control Innate and Adaptive Antiviral Immunity.* J Virol, 2017. **91**(16).
13. Münz, C. and A. Moormann, *Immune escape by Epstein-Barr virus associated malignancies.* Semin Cancer Biol, 2008. **18**(6): p. 381-7.
14. Soldan, S.S. and P.M. Lieberman, *Epstein–Barr virus and multiple sclerosis.* Nature Reviews Microbiology, 2023. **21**(1): p. 51-64.
15. Dukers, D.F., et al., *Direct immunosuppressive effects of EBV-encoded latent membrane protein 1.* J Immunol, 2000. **165**(2): p. 663-70.
16. Middeldorp, J.M. and D.M. Pegtel, *Multiple roles of LMP1 in Epstein-Barr virus induced immune escape.* Seminars in Cancer Biology, 2008. **18**(6): p. 388-396.
17. Liu, S.-C., et al., *Leukemia inhibitory factor promotes nasopharyngeal carcinoma progression and radioresistance.* The Journal of Clinical Investigation, 2013. **123**(12): p. 5269-5283.
18. Kong, A.T., et al., *MSFragger: ultrafast and comprehensive peptide identification in mass*

spectrometry–based proteomics. Nature Methods, 2017. **14**(5): p. 513-520.
19. Love, M.I., W. Huber, and S. Anders, *Moderated estimation of fold change and dispersion for RNA-seq data with DESeq2.* Genome Biol, 2014. **15**(12): p. 550.
20. Subramanian, A., et al., *Gene set enrichment analysis: A knowledge-based approach for interpreting genome-wide expression profiles.* Proceedings of the National Academy of Sciences, 2005. **102**(43): p. 15545.
21. Hao, Y., et al., *Dictionary learning for integrative, multimodal and scalable single-cell analysis.* Nat Biotechnol, 2024. **42**(2): p. 293-304.
22. McGinnis, C.S., L.M. Murrow, and Z.J. Gartner, *DoubletFinder: Doublet Detection in Single-Cell RNA Sequencing Data Using Artificial Nearest Neighbors.* Cell Systems, 2019. **8**(4): p. 329-337.e4.
23. Coulton, A., et al., *Using a pan-cancer atlas to investigate tumour associated macrophages as regulators of immunotherapy response.* Nature Communications, 2024. **15**(1): p. 5665.
24. Hänzelmann, S., R. Castelo, and J. Guinney, *GSVA: gene set variation analysis for microarray and RNA-Seq data.* BMC Bioinformatics, 2013. **14**(1): p. 7.
25. Browaeys, R., W. Saelens, and Y. Saeys, *NicheNet: modeling intercellular communication by linking ligands to target genes.* Nat Methods, 2020. **17**(2): p. 159-162.
26. Duluc, D., et al., *Tumor-associated leukemia inhibitory factor and IL-6 skew monocyte differentiation into tumor-associated macrophage-like cells.* Blood, 2007. **110**(13): p. 4319-30.
27. Viswanadhapalli, S., et al., *Targeting LIF/LIFR signaling in cancer.* Genes Dis, 2022. **9**(4): p. 973-980.
28. Wang, J., et al., *Leukemia inhibitory factor, a double-edged sword with therapeutic implications in human diseases.* Mol Ther, 2023. **31**(2): p. 331-343.
29. Barrett, C.W., et al., *Selenoprotein P influences colitis-induced tumorigenesis by mediating stemness and oxidative damage.* J Clin Invest, 2015. **125**(7): p. 2646-60.
30. Qian, J., et al., *A pan-cancer blueprint of the heterogeneous tumor microenvironment revealed by single-cell profiling.* Cell Research, 2020. **30**(9): p. 745-762.
31. Cheng, S., et al., *A pan-cancer single-cell transcriptional atlas of tumor infiltrating myeloid cells.* Cell, 2021. **184**(3): p. 792-809.e23.
32. Lee, P.-J., et al., *Epstein-Barr viral product-containing exosomes promote fibrosis and nasopharyngeal carcinoma progression through activation of YAP1/FAPα signaling in fibroblasts.* Journal of Experimental & Clinical Cancer Research, 2022. **41**(1): p. 254.
33. Liu, S.C., et al., *Epstein-Barr Virus Induces Adipocyte Dedifferentiation to Modulate the Tumor Microenvironment.* Cancer Res, 2021. **81**(12): p. 3283-3294.

Acknowledgements

This work was funded by the National Science and Technology Council, Taiwan (112-2314-B-008 -001 -MY3 and 109-2314-B-008-001-MY3). Ethics approval and consent to participate this study was approved by the Institutional Review Board (IRB 202202095B0 and IRB201801247B0) of Chang Gung Memorial Hospital, Taiwan. Animal studies using mice were approved by the animal committees of National Central University (Taoyuan, Taiwan)

Abbreviations

NPC: Nasopharyngeal carcinoma
EBV: Epstein-Barr virus
LIF: leukemia inhibitory factor
LMP1: latent infection membrane protein 1
EBERs: EBV-encoded small RNAs
Exo: exosome
Mφ: Macrophage
TAMs: tumor-associated macrophages
CAFs: cancer-associated fibroblasts
VEGF: vascular endothelial growth factor
FFPE: formalin-fixed paraffin-embedded
FBS: fetal bovine serum
P/S: penicillin-streptomycin
TEM: transmission electron microscopy
BSA: bovine serum albumin
PCA: principal component analysis
RNA-seq: RNA Sequencing
scRNA-seq: Single-cell RNA sequencing
qRT-PCR: quantitative reverse transcription polymerase chain reaction
MS: mass spectrometry
LC-ESI-MS/MS: Liquid Chromatography Electrospray Ionization Tandem Mass Spectrometry
PBMC: Peripheral blood mononuclear cells
RBC: red blood cells
PMA: phorbol 12-myristate 13-acetate
RTCA: real-time analyzer
CM: condition medium
dpf: day post fertilization
GSVA: Gene Set Variation Analysis
NES: normalized enrichment score
IFN: Interferon:

DC: Dendritic cell
Mono: Monocyte
CTLs: cytotoxic T cells
Ag Pres.: Antigen presentation
Pro-inflam.: Pro-inflammatory
Immune Reg: Immune regulatory
TLR: Toll-like receptor
FDR: false discovery rate
MsigDB: The Molecular Signatures Database
WT: wild-type
CMV: cytomegalovirus
ΔCTerm: C-terminally deleted
CTARs: c-terminal activating regions
IHC: Immunohistochemistry
ISH: In situ hybridization
EdU: 5-Ethynyl-2-deoxyuridine
DEGs: differentially expressed genes
IPA: Ingenuity Pathway Analysis
FCGR3A: Fc Gamma Receptor IIIa
UMAP: Uniform manifold approximation and projection

Figure legends

Fig 1. LIF expression correlates with poor prognosis in NPC

(A) Kaplan–Meier survival curves of NPC patients stratified by LIF IHC scores (B) LIF expression in non-metastasis and metastasis patients based on IHC scores (chi-square test). Meta, metastasis. (C) Representative IHC image of PLIF in human NPC tumor. Scale bar, 50μm. (D) Representative immunofluorescence images showing co-localization of LIF (red) and CD68 (green) in human NPC sections. The upper panel shows macrophages in the tumor periphery, while the lower panel shows macrophages within the tumor core, Nuclei stained with Hoechst in blue. Scale bar, 20μm; enlarged images: 2μm. T, tumor.

Fig 2. Detection of EBV-encoded products in human NPC tumors

(A) Representative images of EBV-encoded small RNAs (EBERs), early antigen D (EaD) and LMP1 expression in human NPC tissue sections. Scale bar, 50μm. The detection of EBERs was used by in situ hybridization; EaD and LMP1 were detected by IHC. (B) Images of $EBERs^+$ vesicle-like structures extended from $EBER^+$ NPC tumors Scale bar, 50μm (left), 20μm (right). (C) IHC staining of LMP1 in both the adjacent normal and the cancer regions in human NPC sections. Scale bar, 100μm; enlarged images: 20 μm. (D) Representative immunofluorescence images showing co-localization of LMP1 (red) and CD68 (green) in NPC sections. Nuclei stained with Hoechst in blue. Scale bar, 20μm (upper); 5μm (lower)

Fig 3. EBV-encoded LMP1 is transferred via cancer-derived exosome

(A) TEM images of exosomes captured by immunomagnetic beads coated with antibody against CD9. Arrows indicated captured exosomes. Scale bars, 200 nm. (B) Western blot analysis. Exosomes derived from EBV^+-NPC cells (HK1 EBV) contains EBV latent membrane protein 1 (LMP1) and exosomal markers (CD9 and HSP70). B95.8-derived cell lysates and exosomes were used as positive controls for EBV-encoded products. BM1 was EBV negative control. GAPDH and β-actin were negative control of exosomes. (C) Time-lapse monitoring of exosome uptake by a macrophage at 5 hours post addition of exosomes. Exosomes were pre-labeled with ExoGlow-Protein EV Labeling Kit (green). Scale bars, 10 μm. (D) Representative immunofluorescence images showing co-localization of LMP1 (red) and CD68 (green) human primary PBMCs-derived macrophages. Nuclei stained with Hoechst in blue. Scale bar, 20μm. (E) qRT-PCR analysis showing the expression of EBV transcripts in human primary macrophages. ND: Not Detected. *, p-value <0.05.

Fig 4. NPC-derived exosomes induce macrophage immunosuppressive polarization and cancer cell growth

(A) Morphological changes in macrophages undergone differential polarization processes. Monocytes from human primary PBMCs were differentiated into macrophages and polarized to subtypes by treating cells with various factors or exosomes. Scale bar, 50μm. (B) Principal component analysis

(PCA) of bulk RNA-seq data. RNA was extracted at day12 of the differentiation. (C) RNA-seq analysis revealing expression level of M1-like, M2-like, markers, antigen-presenting and interferon signaling genes in each subtype. Colors represented log2 fold change of mock macrophage. (D, E) qRT-PCR (D) and western blotting (E) analyses showing the expression of M1-like and M2-like markers in macrophages. For qRT-PCR, all dCq were normalized to mock macrophage, with ACTB as an internal control. GAPDH was used as a loading control in western blotting. (F) Phagocytic analysis of human primary macrophages cocultured with primary cancer cells (red arrows). Cancer cells were added into cultures post macrophage differentiation (t=0). Scale bars, 50μm. (G) The growth of NPC cells was measured by RTCA assay. The arrow indicates the time of condition medium addition. Values represent the mean and standard deviation of three replicates. (H) EdU incorporation analysis. TW06 cells were treated with supernatants from macrophages or control medium for 14 hrs. EdU labeling (green) was applied for an advanced 4 hrs. Blue was stained for nuclei. Scale bars, 50μm. Mφ, macrophage. IFN, interferon. CM, condition medium. *, p-value <0.05; **, p-value <0.01; ***, p- value <0.001 (Bonferroni's multiple comparison test).

Fig 5. LIF is associated with the immunosuppressive polarization of TAMs by EB product-containing exosomes

(A) Exosome treatment on human PBMCs-derived macrophages enhances LIF expression via NF-κB signaling. GAPDH was loading control. (B) Activation of LIF through CTAR1 domain of LMP1. Macrophages differentiated from THP-1 were transfected with LMP1-WT or LMP1 mutant plasmids. Total cell lysates (TCL) were collected 36 hours after transfection. GAPDH served as a loading control. (C, D) RTCA analysis showing that depletion of LIF through the addition of sLIFR suppressed Exo-Tx $M\varphi^{CM}$-mediated NPC cell proliferation. (E) Schematic illustration of the zebrafish embryonic xenograft model. NPC cells expressing RFP were injected to into the yolk sac of transgenic (Tg, flila: EGFP) zebrafish embryos. Cancer cells were treated with or without condition medium and sLIFR prior to injection. (F) Representative images of tumor formation and metastasis-like structures spreading through the vasculature (green). Arrows indicate the dissemination sites of metastasis-like structures. (G) Quantification of tumor xenograft area (left) and metastasis-like structures. Each dot represents a single fish embryo. Mφ, macrophage. Tx, treatment. CM, condition medium. Meta, metastasis. dpf, day post fertilization. *, p-value <0.05; **, p-value <0.01; ***, p- value <0.001 (Bonferroni's multiple comparison test).

Fig 6. Single-cell transcriptomic analysis uncovered microenvironment remodeled by NPC-derived exosomes

(A) UMAP visualization of 14,446 qualified single cells. Cells were isolated from human NPC tissue and treated with or without exosomes from EBV^{+} NPC cell lines (HK1EBV exo). Each dot represents a single cell, coloured by annotated cell type. (B) Dot plot showing marker gene expression levels for distinct cell types. (C) UMAP plot of myeloid cells grouped into six subtypes. (D) Differential

expression genes related to specific biological functions. Colors and dot size refer to log2-fold difference and -logP-val, respectively. (E) The proportion of TAM subpopulations relative to the total number of TAMs in each sample. (F) Ingenuity pathway analysis (IPA) revealed several pathways regulated by exosomes in TAMs. Pathways were ranked by activation score (z-score). (G) Violin plots depicting signatures scores in TAMs. Scores were calculated by UCELL method (upper) and GSVA (lower) based on the expression of relevant genes. Each dot indicates a cell. Statistical significance was assessed by paired t-test. TAMs, Tumor-associated macrophages. DC, Dendritic cell. Mono, Monocyte. Ag Pres, Antigen presentation. Pro-inflam, Pro-inflammatory. Immune Reg, Immune regulatory. TLR, Toll-like receptor. *, p-value <0.05; **, p-value <0.01; ***, p- value <0.001 (paired Mann–Whitney *U* test).

Fig 7. EBV$^+$ NPC exosomes induce an immunosuppressive microenvironment

(A) Significantly dysregulated hallmark gene sets in malignant cells identified by GSVA. Pathways are presented in red (upregulated in Exo-Tx group) or blue (downregulated). (B) Ridge plot showing the density of LMP1 UMI count distributions in malignant cells. (C) NicheNet cell-cell communication analysis predicts HSPE1 in T cells as a potential target influenced by ligands released from cancer cells or TAMs. Ligand and target gene activities were calculated based on the interactions between cancer cells and TAMs (ligand sender) and T cells (receiver). (D) Violin plot showing the expression level of HSPE1 in Tregs. (E) Differential expression genes related to specific T cell functions. Colors and dot size refer to log2-fold difference and -logP-val, respectively. (F) GSVA reveals differences in the enrichment between the two groups. Each dot indicates an enrichment score (ES) for a cell. Statistical significance was assessed using paired t-test. TAMs, Tumor-associated macrophages. AUPR, area under the precision-recall curve. LFC, log fold change. Co-stimu, Co-stimulatory. Immune Reg, Immune regulatory. TCR, T cell receptor. CTL, cytotoxic lymphocyte. ES, enrichment score. *, p-value <0.05; **, p-value <0.01; ***, p- value <0.001 (paired Mann–Whitney U test).

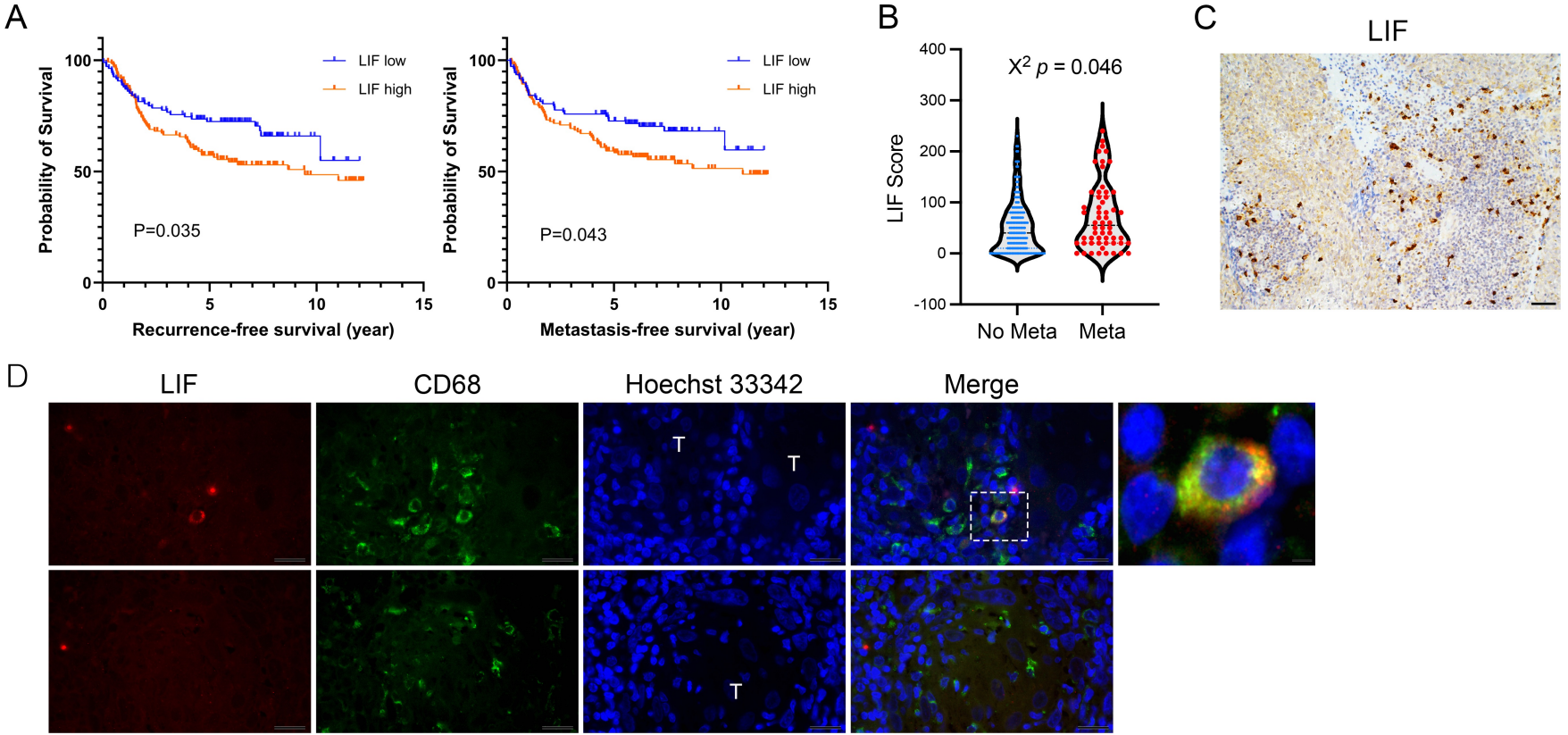
A
LIF low
LIF high
Probability of Survival
100
50
0
P=0.035
0
5
10
15
Recurrence-free survival (year)
LIF low
LIF high
Probability of Survival
100
50
0
P=0.043
0
5
10
15
Metastasis-free survival (year)
B
X2 p = 0.046
LIF Score
400
300
200
100
0
-100
No Meta
Meta
C
LIF
D
LIF
CD68
Hoechst 33342
Merge
T
T
T

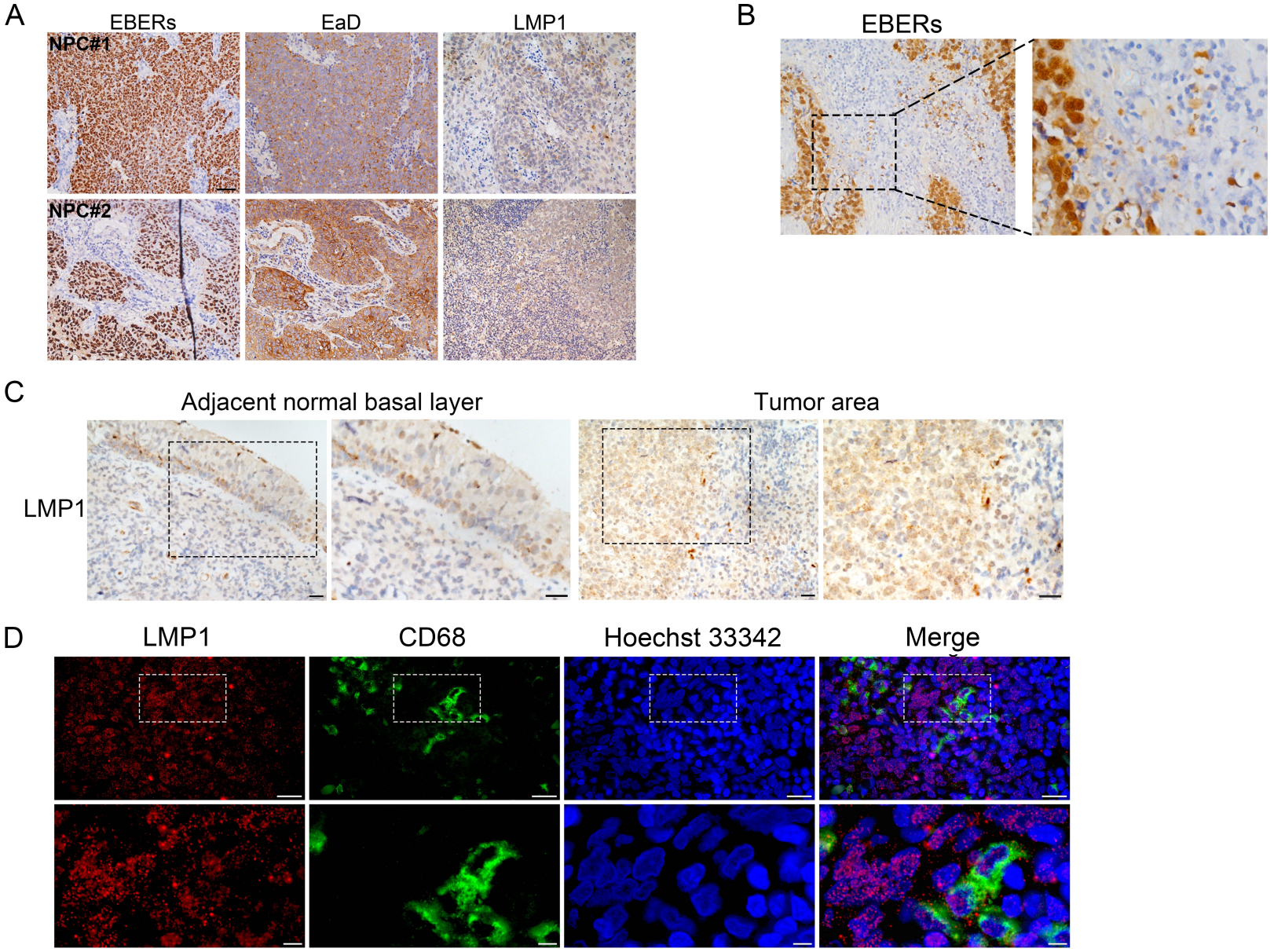
A
EBERs
EaD
LMP1
NPC#1
NPC#2
B
EBERs
C
Adjacent normal basal layer
Tumor area
LMP1
D
LMP1
CD68
Hoechst 33342
Merge

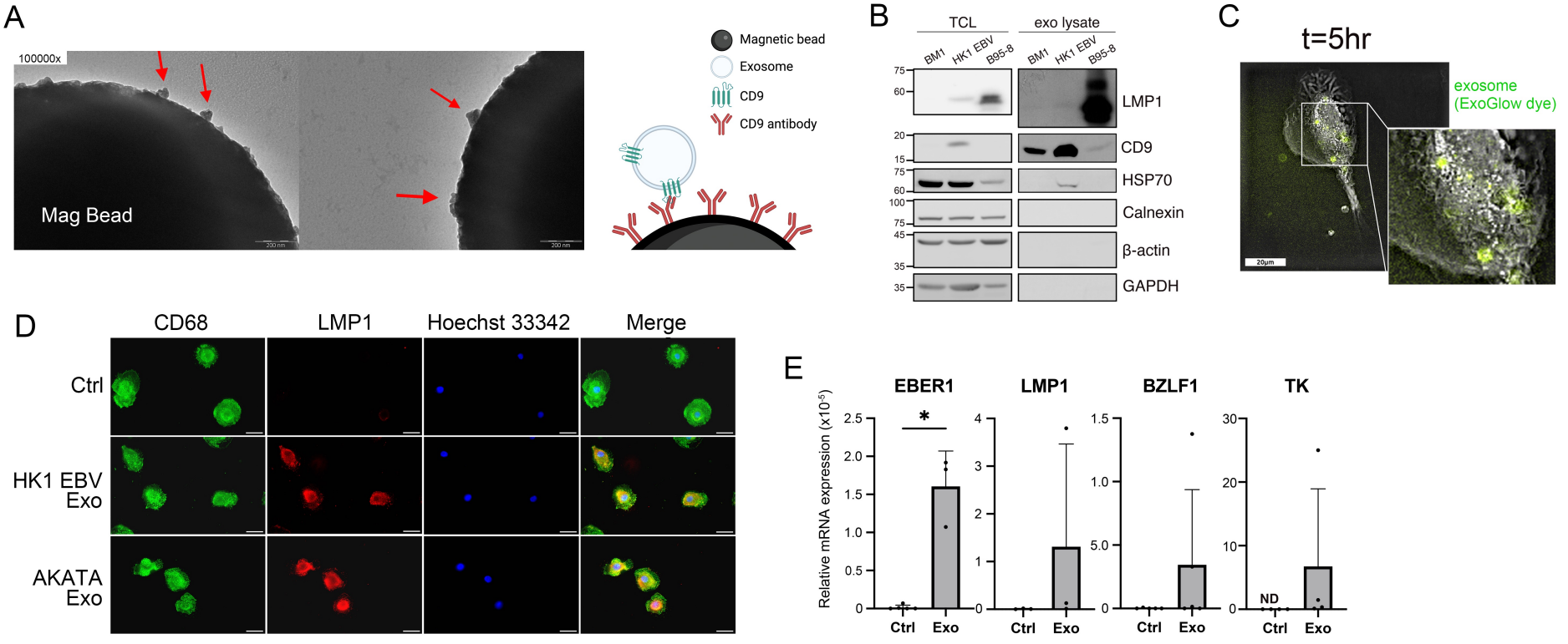
A
100000x
Mag Bead
Magnetic bead
Exosome
CD9
CD9 antibody
B
TCL
exo lysate
BM1
HK1 EBV
B95-8
LMP1
CD9
HSP70
Calnexin
β-actin
GAPDH
C
t=5hr
exosome
(ExoGlow dye)
D
CD68
LMP1
Hoechst 33342
Merge
Ctrl
HK1 EBV Exo
AKATA Exo
E
EBER1
LMP1
BZLF1
TK
Relative mRNA expression (x10⁻⁵)
Ctrl
Exo
ND

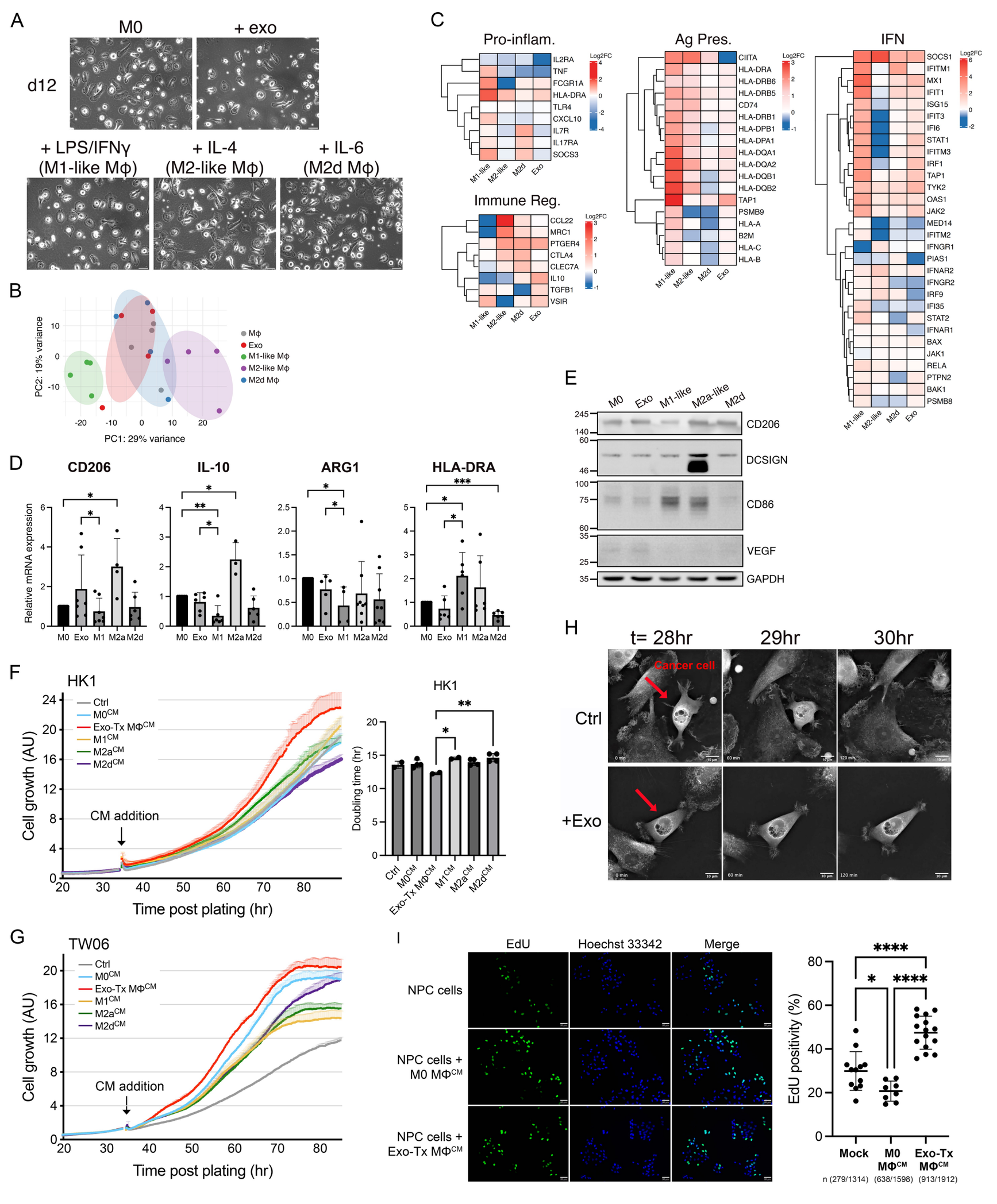
A
M0
+ exo
d12
+ LPS/IFNγ (M1-like Mϕ)
+ IL-4 (M2-like Mϕ)
+ IL-6 (M2d Mϕ)
B
PC2: 19% variance
PC1: 29% variance
Mϕ
Exo
M1-like Mϕ
M2-like Mϕ
M2d Mϕ
C
Pro-inflam.
Ag Pres.
IFN
Immune Reg.
Log2FC
M1-like
M2-like
M2d
Exo
D
CD206
IL-10
ARG1
HLA-DRA
Relative mRNA expression
M0 Exo M1 M2a M2d
E
M0 Exo M1-like M2a-like M2d
CD206
DCSIGN
CD86
VEGF
GAPDH
F
HK1
Cell growth (AU)
Time post plating (hr)
CM addition
Ctrl
M0CM
Exo-Tx MΦCM
M1CM
M2aCM
M2dCM
Doubling time (hr)
G
TW06
H
t= 28hr
29hr
30hr
Cancer cell
Ctrl
+Exo
I
EdU
Hoechst 33342
Merge
NPC cells
NPC cells + M0 MΦCM
NPC cells + Exo-Tx MΦCM
EdU positivity (%)
Mock
M0 MΦCM
Exo-Tx MΦCM
n (279/1314) (638/1598) (913/1912)

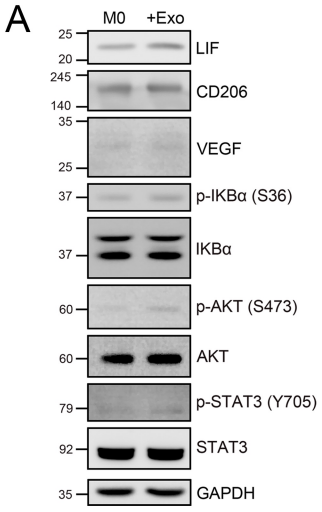
A
M0
+Exo
LIF
CD206
VEGF
p-IKBα (S36)
IKBα
p-AKT (S473)
AKT
p-STAT3 (Y705)
STAT3
GAPDH

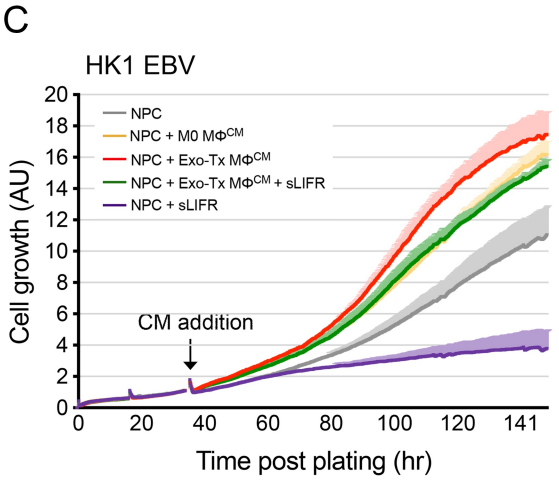
C
HK1 EBV
NPC
NPC + M0 MΦ^CM
NPC + Exo-Tx MΦ^CM
NPC + Exo-Tx MΦ^CM + sLIFR
NPC + sLIFR
CM addition
Cell growth (AU)
Time post plating (hr)

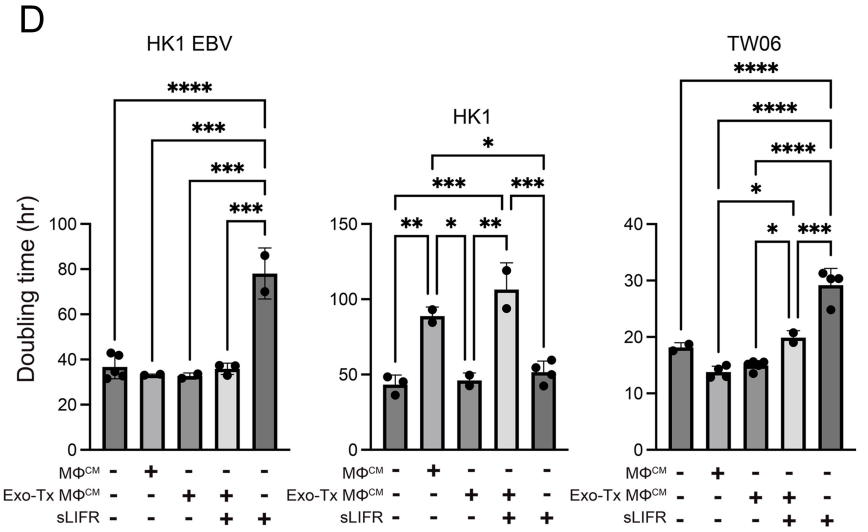
D
HK1 EBV
HK1
TW06
Doubling time (hr)
MΦ^CM
Exo-Tx MΦ^CM
sLIFR

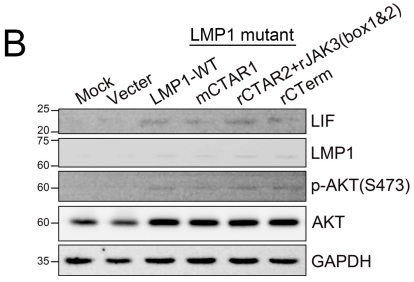
B
LMP1 mutant
Mock
Vecter
LMP1-WT
mCTAR1
rCTAR2+rJAK3(box1&2)
rCTerm
LIF
LMP1
p-AKT(S473)
AKT
GAPDH

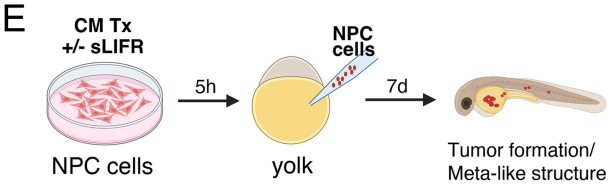
E
CM Tx
+/- sLIFR
5h
NPC cells
7d
NPC cells
yolk
Tumor formation/
Meta-like structure

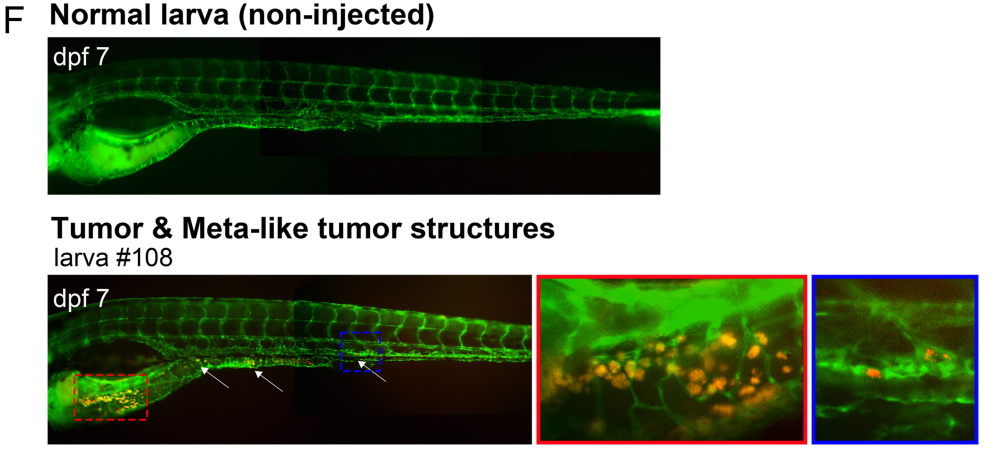
F
Normal larva (non-injected)
dpf 7
Tumor & Meta-like tumor structures
larva #108
dpf 7

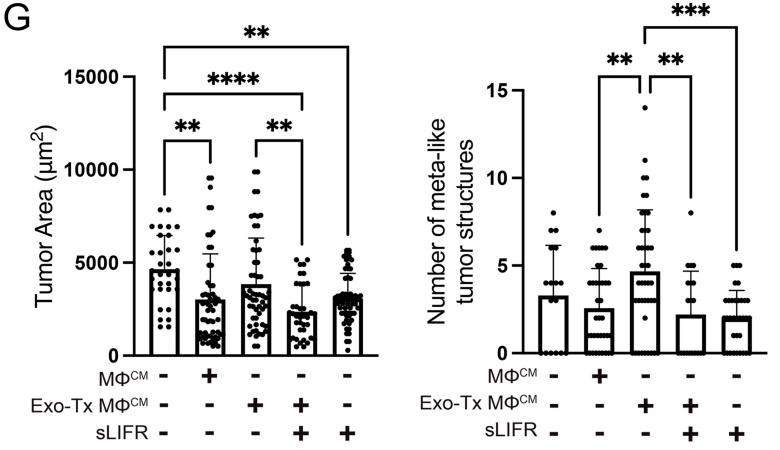
G
Tumor Area (μm²)
Number of meta-like tumor structures
MΦ^CM
Exo-Tx MΦ^CM
sLIFR

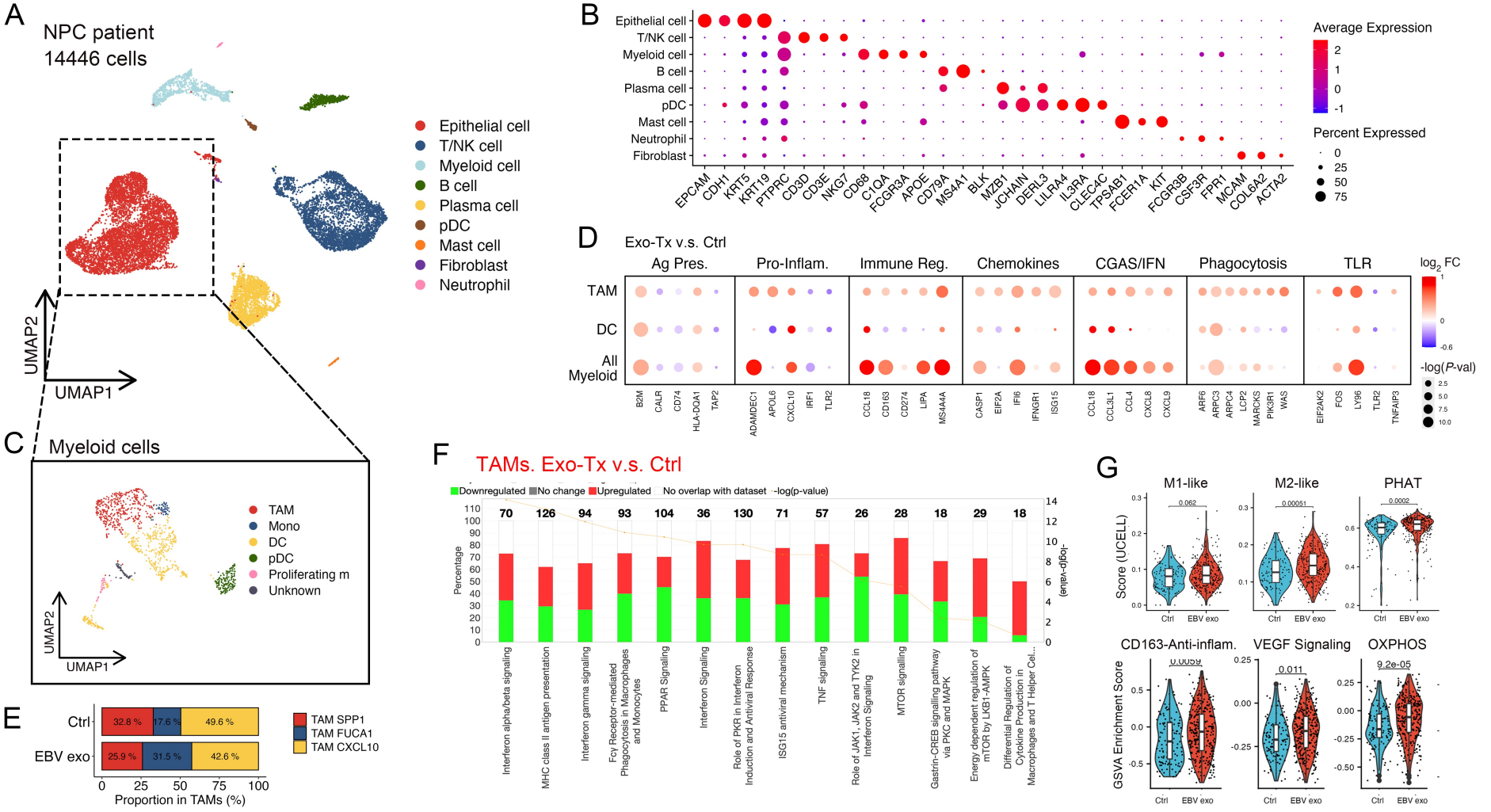
A
NPC patient
14446 cells
Epithelial cell
T/NK cell
Myeloid cell
B cell
Plasma cell
pDC
Mast cell
Fibroblast
Neutrophil
UMAP2
UMAP1
B
Epithelial cell
T/NK cell
Myeloid cell
B cell
Plasma cell
pDC
Mast cell
Neutrophil
Fibroblast
EPCAM CDH1 KRT5 KRT19 PTPRC CD3D CD3E NKG7 CD68 C1QA FCGR3A APOE CD79A MS4A1 BLK MZB1 JCHAIN DERL3 LILRA4 IL3RA CLEC4C TPSAB1 FCER1A KIT FCGR3B CSF3R FPR1 MCAM COL6A2 ACTA2
Average Expression
2
1
0
-1
Percent Expressed
0
25
50
75
C
Myeloid cells
TAM
Mono
DC
pDC
Proliferating m
Unknown
UMAP2
UMAP1
D
Exo-Tx v.s. Ctrl
Ag Pres.
Pro-Inflam.
Immune Reg.
Chemokines
CGAS/IFN
Phagocytosis
TLR
TAM
DC
All Myeloid
B2M CALR CD74 HLA-DQA1 TAP2
ADAMDEC1 APOL6 CXCL10 IRF1 TLR2
CCL18 CD163 CD274 LIPA MS4A4A
CASP1 EIF2A IFI6 IFNGR1 ISG15
CCL18 CCL3L1 CCL4 CXCL8 CXCL9
ARF6 ARPC3 ARPC4 LCP2 MARCKS PIK3R1 WAS
EIF2AK2 FOS LY96 TLR2 TNFAIP3
log2 FC
1
0
-0.6
-log(P-val)
2.5
5.0
7.5
10.0
E
Ctrl
EBV exo
32.8 %
17.6 %
49.6 %
25.9 %
31.5 %
42.6 %
0
25
50
75
100
Proportion in TAMs (%)
TAM SPP1
TAM FUCA1
TAM CXCL10
F
TAMs. Exo-Tx v.s. Ctrl
Downregulated
No change
Upregulated
No overlap with dataset
-log(p-value)
Percentage
70 126 94 93 104 36 130 71 57 26 28 18 29 18
Interferon alpha/beta signaling
MHC class II antigen presentation
Interferon gamma signaling
Fcγ Receptor-mediated Phagocytosis in Macrophages and Monocytes
PPAR Signaling
Interferon Signaling
Role of PKR in Interferon Induction and Antiviral Response
ISG15 antiviral mechanism
TNF signaling
Role of JAK1, JAK2 and TYK2 in Interferon Signaling
MTOR signalling
Gastrin-CREB signalling pathway via PKC and MAPK
Energy dependent regulation of mTOR by LKB1-AMPK
Differential Regulation of Cytokine Production in Macrophages and T Helper Cel...
G
M1-like
M2-like
PHAT
Score (UCELL)
0.062
0.00051
0.0002
Ctrl
EBV exo
CD163-Anti-inflam.
VEGF Signaling
OXPHOS
GSVA Enrichment Score
0.0059
0.011
9.2e-05

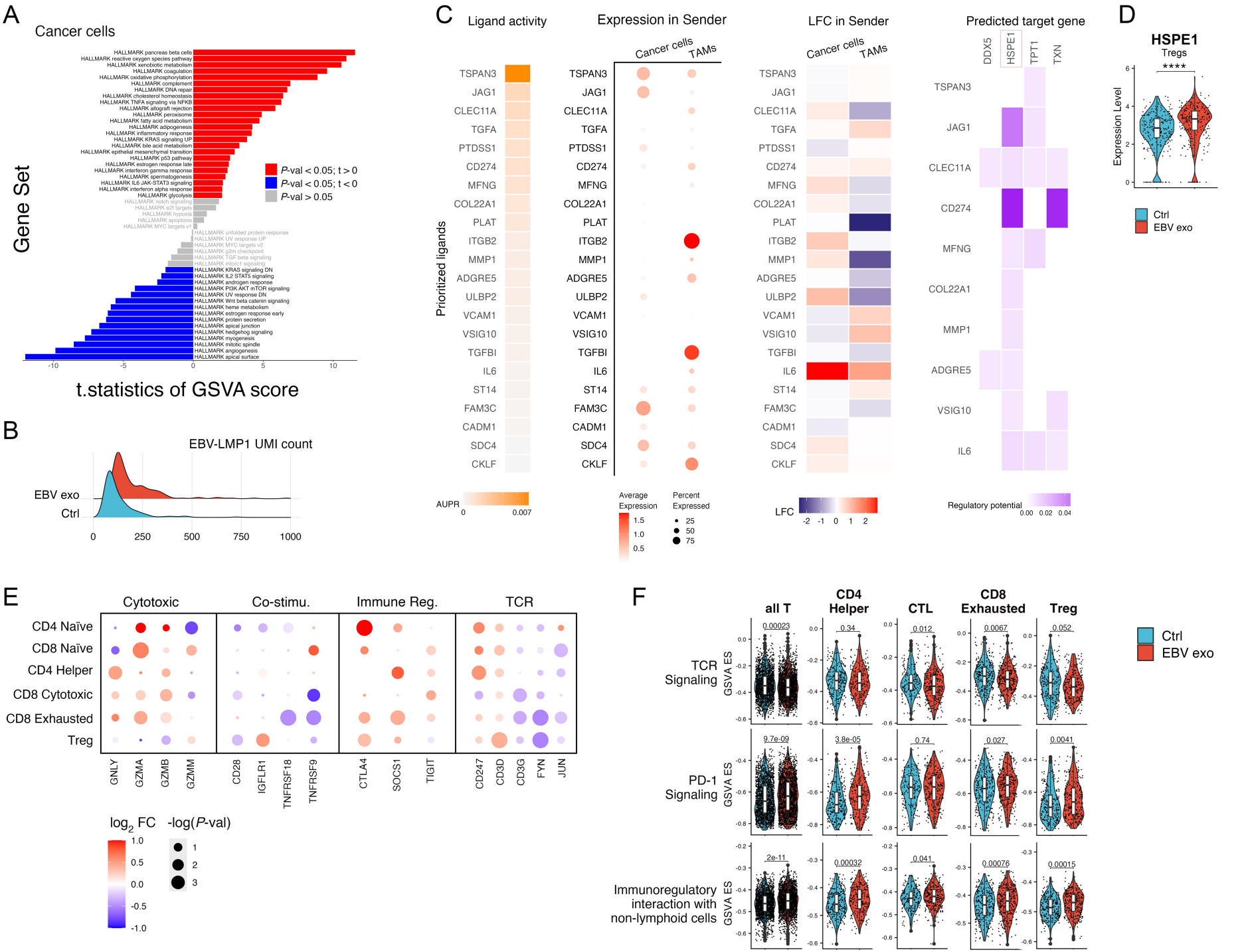
A
Cancer cells
Gene Set
HALLMARK pancreas beta cells
HALLMARK reactive oxygen species pathway
HALLMARK xenobiotic metabolism
HALLMARK coagulation
HALLMARK oxidative phosphorylation
HALLMARK complement
HALLMARK DNA repair
HALLMARK cholesterol homeostasis
HALLMARK TNFA signaling via NFKB
HALLMARK allograft rejection
HALLMARK peroxisome
HALLMARK fatty acid metabolism
HALLMARK adipogenesis
HALLMARK inflammatory response
HALLMARK KRAS signaling UP
HALLMARK bile acid metabolism
HALLMARK epithelial mesenchymal transition
HALLMARK p53 pathway
HALLMARK estrogen response late
HALLMARK interferon gamma response
HALLMARK spermatogenesis
HALLMARK IL6 JAK STAT3 signaling
HALLMARK interferon alpha response
HALLMARK glycolysis
HALLMARK notch signaling
HALLMARK e2f targets
HALLMARK hypoxia
HALLMARK apoptosis
HALLMARK MYC targets v1
HALLMARK unfolded protein response
HALLMARK UV response UP
HALLMARK MYC targets v2
HALLMARK g2m checkpoint
HALLMARK TGF beta signaling
HALLMARK mtorc1 signaling
HALLMARK KRAS signaling DN
HALLMARK IL2 STAT5 signaling
HALLMARK androgen response
HALLMARK PI3K AKT mTOR signaling
HALLMARK UV response DN
HALLMARK Wnt beta catenin signaling
HALLMARK heme metabolism
HALLMARK estrogen response early
HALLMARK protein secretion
HALLMARK apical junction
HALLMARK hedgehog signaling
HALLMARK myogenesis
HALLMARK mitotic spindle
HALLMARK angiogenesis
HALLMARK apical surface
P-val < 0.05; t > 0
P-val < 0.05; t < 0
P-val > 0.05
-10
-5
0
5
10
t.statistics of GSVA score
B
EBV-LMP1 UMI count
EBV exo
Ctrl
0
250
500
750
1000
C
Ligand activity
Expression in Sender
LFC in Sender
Predicted target gene
Cancer cells
TAMs
Prioritized ligands
TSPAN3
JAG1
CLEC11A
TGFA
PTDSS1
CD274
MFNG
COL22A1
PLAT
ITGB2
MMP1
ADGRE5
ULBP2
VCAM1
VSIG10
TGFBI
IL6
ST14
FAM3C
CADM1
SDC4
CKLF
DDX5
HSPE1
TPT1
TXN
AUPR
0
0.007
Average Expression
1.5
1.0
0.5
Percent Expressed
25
50
75
LFC
-2
-1
0
1
2
Regulatory potential
0.00
0.02
0.04
D
HSPE1
Tregs
****
Expression Level
Ctrl
EBV exo
E
Cytotoxic
Co-stimu.
Immune Reg.
TCR
CD4 Naïve
CD8 Naïve
CD4 Helper
CD8 Cytotoxic
CD8 Exhausted
Treg
GNLY
GZMA
GZMB
GZMM
CD28
IGFLR1
TNFRSF18
TNFRSF9
CTLA4
SOCS1
TIGIT
CD247
CD3D
CD3G
FYN
JUN
log2 FC
1.0
0.5
0.0
-0.5
-1.0
-log(P-val)
1
2
3
F
all T
CD4 Helper
CTL
CD8 Exhausted
Treg
TCR Signaling
PD-1 Signaling
Immunoregulatory interaction with non-lymphoid cells
GSVA ES
0.00023
0.34
0.012
0.0067
0.052
9.7e-09
3.8e-05
0.74
0.027
0.0041
2e-11
0.00032
0.041
0.00076
0.00015
Ctrl
EBV exo